

自由曲面补偿飞秒激光成丝系统像差的应用

解博夫¹, 赵星^{1,2*}, 陶诗诗¹, 张帅¹, 李浩然¹, 李渊博¹, 刘洪亮^{1,2}, 刘伟伟^{1,2}¹南开大学现代光学研究所, 天津 300350;²天津市微尺度光学信息技术科学重点实验室, 天津 300350

摘要 针对飞秒激光远距离成丝系统所产生的像差, 基于光学自由曲面较强的像差补偿能力, 提出了在飞秒激光成丝系统中使用透射式自由曲面相位板补偿系统像差的方法。首先, 在光学设计软件中对实际系统像差特性进行了仿真建模。然后, 对透射式自由曲面相位板进行了优化设计, 优化后系统的像差得到了有效补偿, 飞秒激光光斑质量得到了改善。最后, 对优化设计后的自由曲面相位板进行了公差分析, 并利用加工后的透射式自由曲面相位板开展了实验研究。结果表明, 飞秒激光聚焦系统引入光学自由曲面相位板后, 聚焦光斑形状规则, 在聚焦位置处光斑的均方根(RMS)半径小于0.5 mm, 飞秒激光成丝系统的像差得到了有效补偿, 远距离飞秒激光的成丝强度得到了有效提高。

关键词 光学设计; 像差补偿; 飞秒激光成丝; 光学自由曲面

中图分类号 O435.2

文献标志码 A

DOI: 10.3788/AOS221720

1 引言

光学自由曲面是指无法采用传统球面或者非球面表达式来描述的曲面, 其在空间上一般具有非旋转对称性。相较于一般的旋转对称曲面, 如球面、二次曲面等, 自由曲面具有较多的设计自由度和较强的像差补偿能力^[1-4], 有时一片自由曲面的光学性能甚至比多片球面或非球面组合好, 大大减小了光学系统的复杂程度和简化了空间布局, 故自由曲面被广泛应用于成像系统和非成像系统中^[5-8]。在成像系统中, 自由曲面主要被应用在头戴显示器^[9-11]、超短焦投影机^[12]、全景光学系统^[13]和离轴三反望远镜系统等大视场、大孔径光学系统中^[14-17]。在这些系统中, 由于视场和孔径过大, 故所引起的像差如球差、像散和畸变等均会增大, 常规的球面或二次曲面需要很复杂的结构组合才能消除像差, 但利用一至两片自由曲面往往便可达到很好的补偿效果。在非成像系统中, 自由曲面往往被应用于聚光和照明系统中^[18-21], 如自由曲面全内反射准直器(TIR)被应用于短焦照明系统中等, 在获得准直均匀照明光源的同时, 还大大提高了能量利用效率。

飞秒激光因其非线性光学效应会在聚焦处形成等离子体通道, 即光丝。飞秒激光成丝系统在遥感探测领域中有诸多应用, 如光丝可用作远距离探测物质成分荧光光谱的激励源^[22-24], 以此实现大气污染物成分和含量监测等功能。然而, 在远距离形成光丝的过程

中, 聚焦系统中存在的各种像差会使得聚焦处光斑形状不规则, 光斑尺寸偏大, 光斑质量下降, 进而导致光丝强度减弱^[25], 降低探测灵敏度。光学自由曲面具有突出的像差补偿能力, 故可以通过在飞秒激光远距离成丝系统中引入自由曲面来补偿系统像差, 提高聚焦时光斑形状规则度, 减小光斑半径, 提升光斑质量, 以获得较强的光丝, 从而提高系统探测灵敏度。

本文针对飞秒激光成丝系统在远距离聚焦成丝时的像差, 提出了使用透射式自由曲面相位板补偿系统像差的方法。首先, 通过光学设计软件搭建出与实际系统具有相同像差特性的仿真系统。然后, 优化引入的透射式自由曲面相位板的面形, 系统的像差得到了有效补偿, 飞秒激光聚焦光斑形状规则度和大小均得到改善。在此基础上, 对优化设计后的自由曲面进行公差分析, 并按照设计结果进行加工。最后, 将加工后的自由曲面置于实验系统中开展实验研究, 结果表明光学自由曲面能够显著补偿飞秒激光成丝系统的像差, 有效提高了远距离飞秒激光的成丝强度。

2 系统仿真

图1为搭建出来的用于800 nm飞秒激光远距离聚焦成丝的系统示意图, 其中f为扩束凹透镜焦距。飞秒激光经反射镜1反射至凹透镜进行扩束, 再由反射镜2经凹面反射镜反射并聚焦于远处。改变平面反射镜1与凹面反射镜之间的距离即可实现在不同距离

收稿日期: 2022-09-20; 修回日期: 2022-10-22; 录用日期: 2022-10-31; 网络首发日期: 2022-11-04

基金项目: 国家重点研发计划(2018YFB0504400)、国家自然科学基金(62075106)

通信作者: *zhaoxingtjnk@nankai.edu.cn

下的聚焦。其中,凹面反射镜采用的是Edmund生产
的高精度抛物面反射镜,其焦距为2032 mm,通光孔径

为412.8 mm,曲率半径为4064 mm。

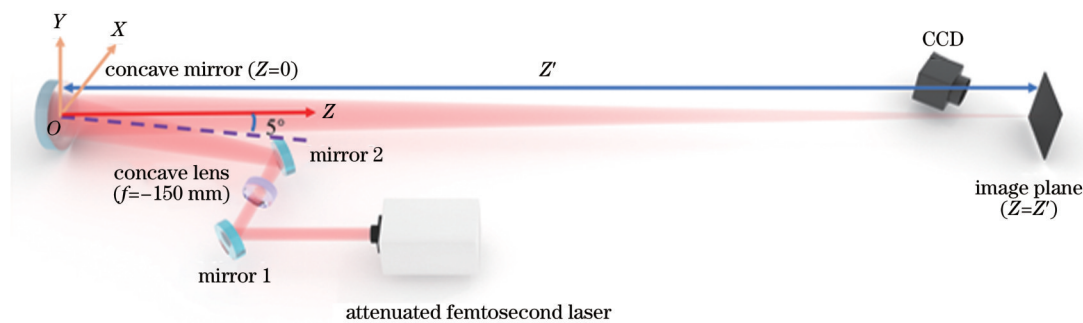


图1 飞秒激光远距离聚焦成丝系统示意图

Fig. 1 Schematic diagram of femtosecond laser long-distance focusing and filamentation system

在光学设计软件CODE V中按照实验系统结构和器件参数建立仿真系统,通过改变像面与凹面反射镜之间的距离,得到不同距离 Z' 下的光斑点列图,以此分析原系统的像差特性。图2为仿真系统示意图,采用数值孔径相同的点光源代替图1中平行光经凹透镜后的发散光束。沿光束传播方向,光源距离平面反

射镜的距离为 $d_1=200$ mm,平面反射镜和凹面反射镜之间的距离为 $d_2=2350.80$ mm,此时光束在 $Z'=10$ m处聚焦,系统详细设计参数如表1所示,波长为800 nm,物方数值孔径为0.059829。图3为距离凹面镜不同距离时,像面处以光斑质心为参考的光斑点列图。

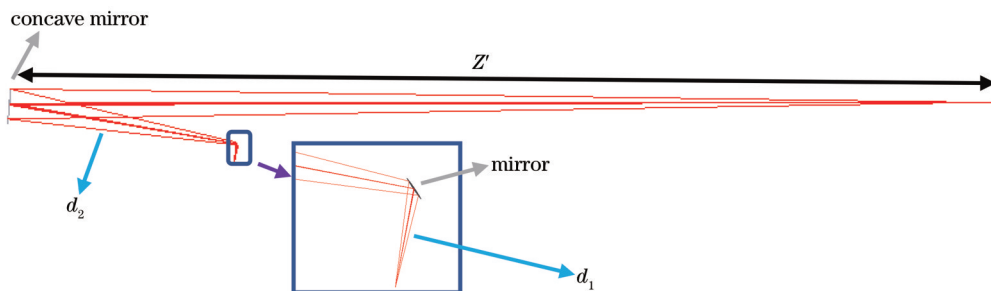


图2 CODE V 仿真飞秒激光在10 m 处聚焦成丝系统示意图

Fig. 2 Schematic diagram of femtosecond laser focusing and filamentation system at 10 m simulated by CODE V

表1 飞秒激光在10 m 聚焦成丝系统详细设计参数

Table1 Detailed design parameters of femtosecond laser focusing and filamentation system at 10 m

Surface	Thickness /mm	Radius /mm	Conic	Semi-diameter /mm	Optical axis deflection angle /($^{\circ}$)
Object	200.00	∞	0		
Mirror	2350.80	∞	0	25.4	90
Concave mirror	10000.00	4064	-1	206.4	10

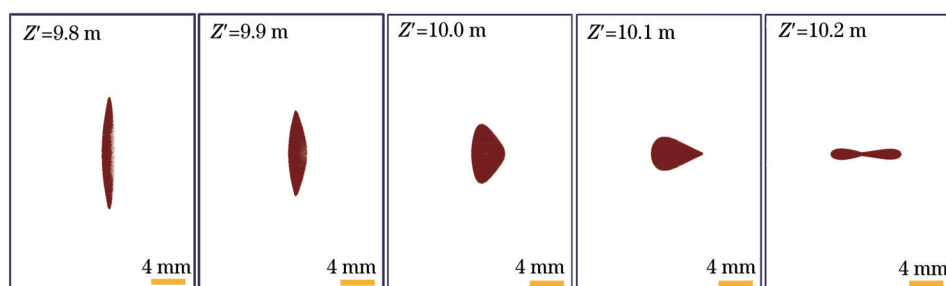


图3 距离凹面镜不同距离时像面处光斑点列图

Fig. 3 Light spot patterns on image plane at different distances from concave mirror

从图3看出:在10 m聚焦位置处,光斑形状不规则且较大;在聚焦位置前后,出现弧矢与子午光束先后会聚的情况。进一步分析可知,10 m聚焦处的波像差峰谷(PV)值为 58.89λ ($\lambda=800 \text{ nm}$),采用16项Fringe Zernike多项式表征该波像差可得如图4所示的各项系数分布,其中第5项X方向像散项系数最大(33λ)。由此可以得出,原系统中波像差总体较大,且存在的主要波像差为X方向像散。另外,从图4中插图所示的光程差(OPD)曲线图也能看出,无论在子午方向还是弧矢方向上,系统均存在较大的波像差。

3 自由曲面相位板优化设计

为了补偿系统中的像差,在系统中平面反射镜与凹面反射镜之间添加一块透射式自由曲面相位板。相位板的材料选用聚甲基丙烯酸甲酯(PMMA),将后表面设置为平面,前表面设置为18项Fringe Zernike型自由曲面,其面形表达式为

$$z(x, y) = \frac{c(x^2 + y^2)}{1 + \sqrt{1 - (1 + k)c^2(x^2 + y^2)}} + \sum_i Z_i \varphi_i(\rho, \varphi), \quad (1)$$

式中:等式右边第一项为基准项,参量 c 和 k 分别表示二次曲面顶点曲率和二次曲面系数;等式右边第二项

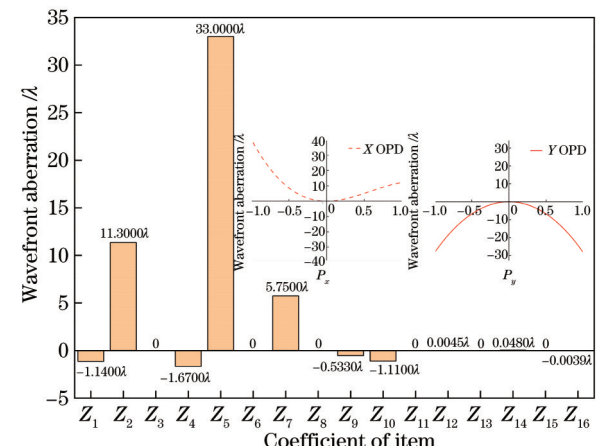


图4 优化前系统波像差分布图

Fig. 4 Wavefront aberration distribution of system before optimization

为Zernike多项式基函数的叠加,其中 Z_i 表示Zernike多项式系数, φ_i 表示第*i*项Zernike多项式, ρ 表示归一化半径, φ 表示方位角。将顶点曲率半径、二次系数项、4~18项Zernike系数、相位板自身厚度和平面与凹面反射镜之间的距离设置为优化变量,以补偿X方向像散并使得系统波像差PV值小于 $\lambda/4$ 为优化目标,满足瑞利判断。优化后的系统示意图和透射式自由曲面相位板各项系数分别如图5和表2所示。

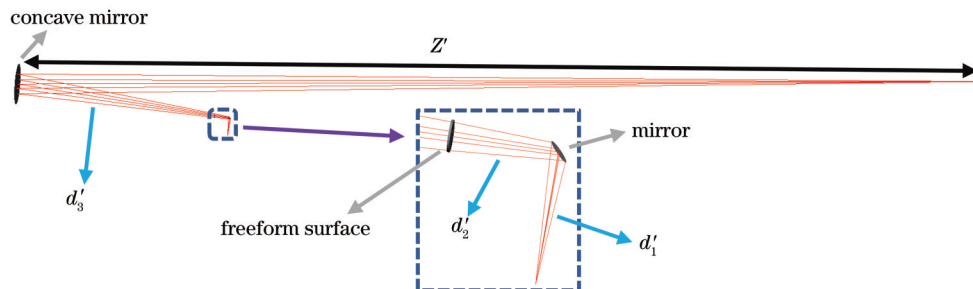


图5 优化后飞秒激光10 m聚焦成丝系统示意图

Fig. 5 Schematic diagram of optimized femtosecond laser focusing and filamentation system at 10 m

在图5中,沿光束传播方向,光源与平面反射镜之间的距离为 $d'_1 = 200 \text{ mm}$,平面反射镜与自由曲面相位板前表面的距离为 $d'_2 = 152.78 \text{ mm}$,自由曲面相位板后表面与凹面镜之间的距离为 $d'_3 = 2046.35 \text{ mm}$ 。

在表2中, T_i 表示透射式自由曲面相位板的厚度, R_i 表示前表面的曲率半径, K_i 表示二次曲面系数, ρ_i 表示自由曲面归一化半径, D_i 表示相位板的通光孔径, $Z_{1t} \sim Z_{1s}$ 表示18项Fringe Zernike的系数。根据以上面形数据,得到的透射式自由曲面相位板前表面的矢高(Sag)图如图6所示。

优化后10 m聚焦位置前后的光斑点列图如图7所示。可以看出:引入自由曲面并经过优化之后,在10 m聚焦处和其前后的光斑形状几乎保持为圆形,相比图3优化之前各位置处的光斑,形状规则度有了极

大改善;优化后由几何像差决定的光斑半径也明显变小,小于艾里斑半径($45 \mu\text{m}$),聚焦效果良好。从图8所示的Finge Zernike表征的10 m聚焦处波像差系数分布图和OPD曲线来看,其第5项X方向像散项系数明显减小,优化后系统的波像差PV值也显著减小至 0.0056λ ,系统最大波像差小于 $\lambda/4$,满足瑞利判据。

上述结果表明,自由曲面有效地补偿了系统像差:当采用球面镜来补偿系统像差时,优化后曲率半径为 -247.80 mm ,系统的波像差PV值为 9.36λ ,聚焦时光斑均方根(RMS)半径为 1 mm ;当采用传统非球面来补偿系统像差时,优化后的曲率半径和二次系数分别为 -246.29 mm 和 -4.56 ,此时系统波像差PV值为 9.07λ ,聚焦时光斑RMS半径为 0.7 mm 。因此,相较于球面和旋转非球面,自由曲面具有非常突出的像

表2 优化后透射式自由曲面相位板面形参数

Table 2 Optimized surface shape parameters of transmission freeform surface phase plate

Parameter	Optimization result	Parameter	Optimization result
T_t/mm	4.0000	Z_{8t}	-1.1840×10^{-8}
R_t/mm	-248.7424	Z_{9t}	-7.3544×10^{-4}
ρ_t/mm	23.0000	Z_{10t}	-2.9977×10^{-4}
D_t/mm	46.0000	Z_{11t}	-4.9952×10^{-9}
K_t	-3.6893	Z_{12t}	-2.6967×10^{-5}
Z_{1t}	0	Z_{13t}	-9.5429×10^{-9}
Z_{2t}	0	Z_{14t}	1.2820×10^{-5}
Z_{3t}	0	Z_{15t}	-7.9483×10^{-9}
Z_{4t}	0.2995	Z_{16t}	2.9688×10^{-6}
Z_{5t}	0.0267	Z_{17t}	3.9446×10^{-6}
Z_{6t}	1.2350×10^{-9}	Z_{18t}	3.8836×10^{-9}
Z_{7t}	-3.6480×10^{-3}		

差补偿能力。

4 公差分析

在第3章透射式自由曲面相位板设计结果的基础上,考虑到后续加工误差和实验过程中装调误差对最终聚焦光斑大小的影响,需要对设计结果进行加工误差和装调误差的公差分析。厂家给出加工的面形误差为PV值小于1 μm,或者对应于表面RMS误差约为

$0.3\lambda(\lambda=546.1\text{ nm})$ 。相位板装调误差包括沿X、Y、Z三个方向的偏心误差和倾斜误差。

利用光学设计软件中Monte Carlo公差分析模块对系统进行公差分析。加工误差由厂家给出的表面RMS误差值决定。装调公差包括的倾斜与偏心公差的数值由实验中调节器件的精度决定,公差类型及其对应数值如表3所示。

根据表3中的公差类型和对应的数值,以聚焦光斑的RMS直径为公差分析结果的性能衡量参量,对透射式自由曲面相位板进行100次Monte Carlo实验分析,其分析结果的概率分布图如图9所示。

从图9的公差分析结果可以看出,透射式自由曲面相位板在面形公差和装调公差双重影响下,飞秒激光聚焦系统的光斑RMS直径有97.7%的概率不超过0.4598 mm,仍然保持着较好的聚焦效果。

5 像差补偿实验研究

采用单点金刚石车削的方式将透射式自由曲面相位板按照设计结果进行加工,结果如图10所示,在样品通光孔径范围之外添加了装调定位孔。

5.1 面形检测

采用ZYGO NewView™ 9000三维光学轮廓仪对透射式自由曲面相位板表面矢高进行扫描检测,选择过自由曲面几何中心的水平方向和竖直方向的表面矢高与仿真设计结果进行对比。从图11看到,在扫描的

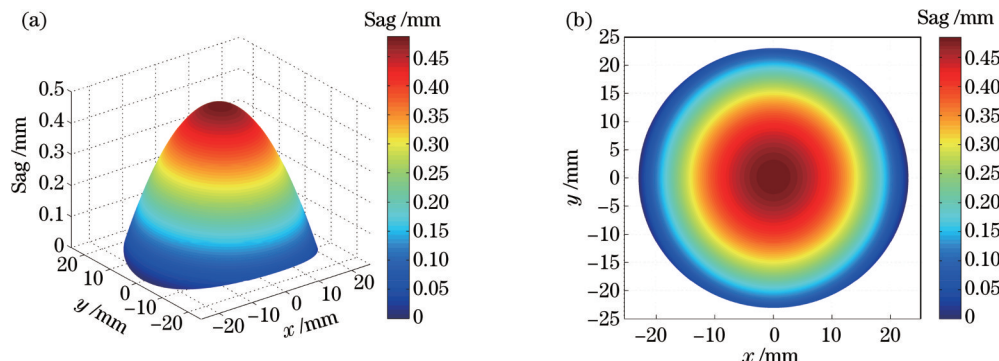


图6 透射式自由曲面相位板面形矢高图。(a)三维图;(b)俯视图

Fig. 6 Surface shape Sag diagram of transmission freeform phase plate. (a) Three-dimensional diagram; (b) vertical view

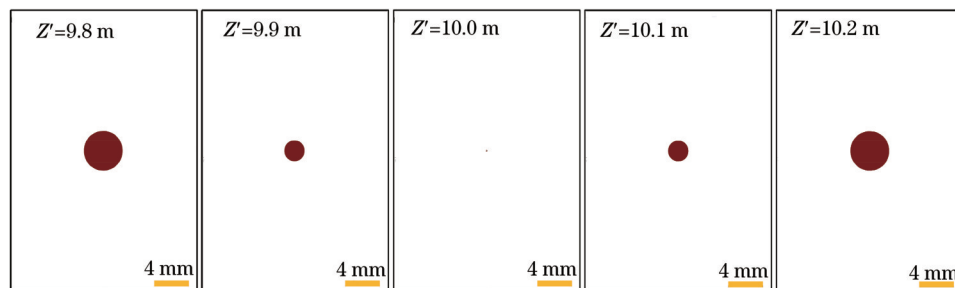


图7 优化后距离凹面镜不同距离时像面处光斑点列图

Fig. 7 Light spot patterns on image plane at different distances from concave mirror after optimization

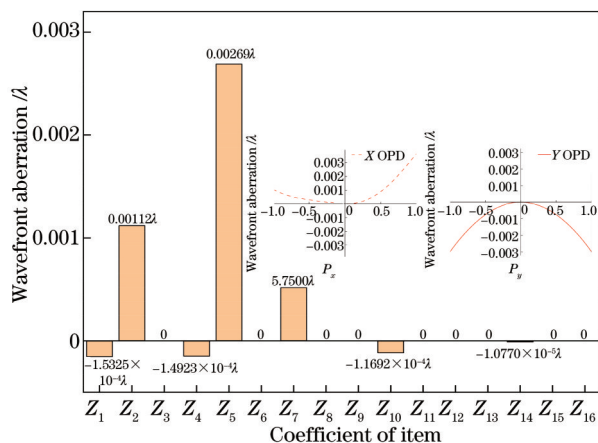


图8 优化后系统波像差分布图

Fig. 8 Wavefront aberration distribution of system after optimization

表3 透射式自由曲面相位板公差类型及其对应数值

Table 3 Tolerance types and corresponding values of transmission freeform surface phase plate

Tolerance type	Component	CODE V macro command	Value
Surface tolerance	RMS error	RSE($\lambda = 546.1 \text{ nm}$)	0.3000
Tilt tolerance	α	DLA	$3.4000 \times 10^{-3} \text{ rad}$
	β	DLB	$5.8100 \times 10^{-4} \text{ rad}$
	γ	DLG	$3.4000 \times 10^{-3} \text{ rad}$
Decenter tolerance	ΔX	DLX	1.0000 mm
	ΔY	DLY	1.0000 mm
	ΔZ	DLZ	1.0000 mm

口径范围内,与设计结果相比,相位板水平方向和垂直

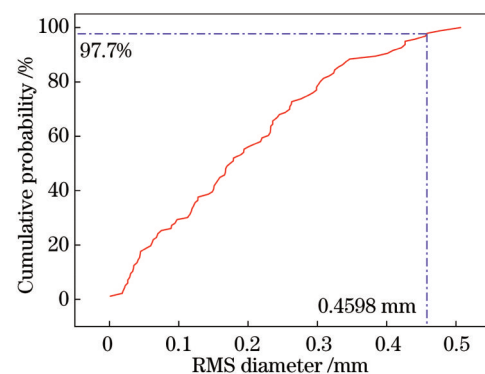


图9 Monte Carlo公差分析得到的光斑RMS直径变化概率图

Fig. 9 Probability diagram of light spot RMS diameter change obtained by Monte Carlo tolerance analysis

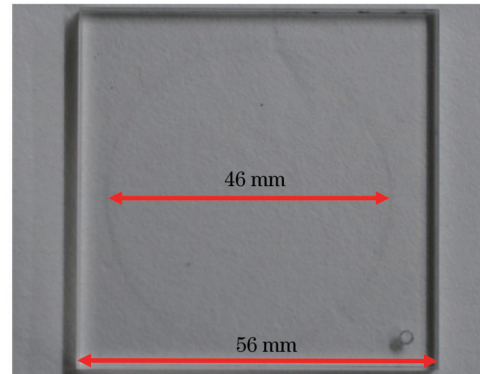


图10 透射式自由曲面相位板实物图

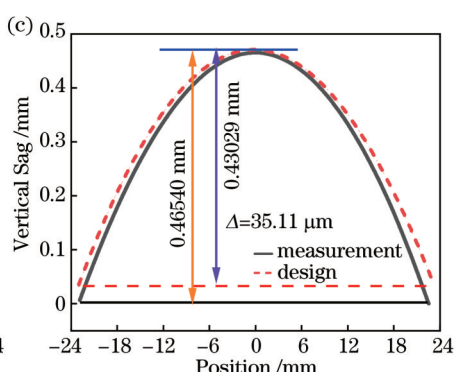
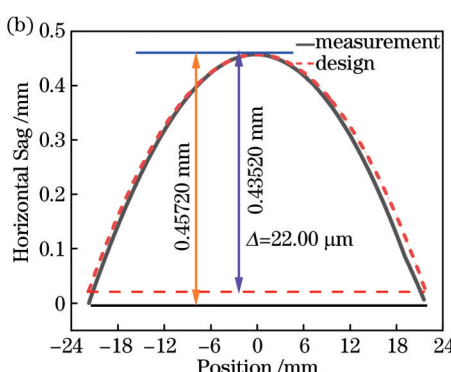
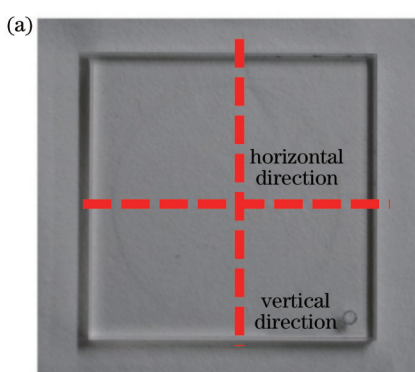
Fig. 10 Physical drawing of transmission freeform phase plate
方向的口径边缘矢高加工误差 Δ 分别为 $22.00 \mu\text{m}$ 和 $35.11 \mu\text{m}$,并未达到预期的面形加工精度。

图11 透射式自由曲面相位板水平方向和竖直方向设计矢高与扫描结果对比。(a)水平方向和竖直方向示意图;(b)水平方向设计矢高与扫描结果对比;(c)竖直方向设计矢高与扫描结果对比

Fig. 11 Comparison of design Sag and scanning result of transmission freeform surface phase plate in horizontal and vertical directions.
(a) Schematic diagram for horizontal and vertical directions; (b) comparison of design Sag and scanning result in horizontal direction; (c) comparison of design Sag and scanning result in vertical direction

由于自由曲面具有非旋转对称性,故准确扫描得出全口径下面形矢高结果的难度很大,但可将上述水平方向和竖直方向的矢高加工误差转化为面形曲率半

径变化,以此来半定量化分析加工误差对系统聚焦效果的影响。从光学设计软件中得到边缘孔径处矢高变化与曲率半径变化之间的对应关系为

$$\Delta S = -\Delta r \frac{D^2}{8r^2}, \quad (2)$$

式中: D 表示镜面直径; ΔS 表示边缘孔径矢高改变量; Δr 表示曲率半径改变量; r 表示原始曲率半径。不考虑装调误差时: 水平方向上边缘孔径处矢高改变量约为 $22 \mu\text{m}$, 对应曲率半径改变量约为 5.15 mm , 光线追

迹得到的聚焦位置将前移至距凹面镜 9.8420 m 处; 坚直方向上边缘孔径处矢高改变量约为 $35 \mu\text{m}$, 对应曲率半径改变量约为 7.59 mm , 光线追迹得到的聚焦位置将会前移至距凹面镜 9.7680 m 处。图 12 展示了分别在水平方向和坚直方向矢高误差影响下聚焦处前后 0.4 m 范围内的光斑图。

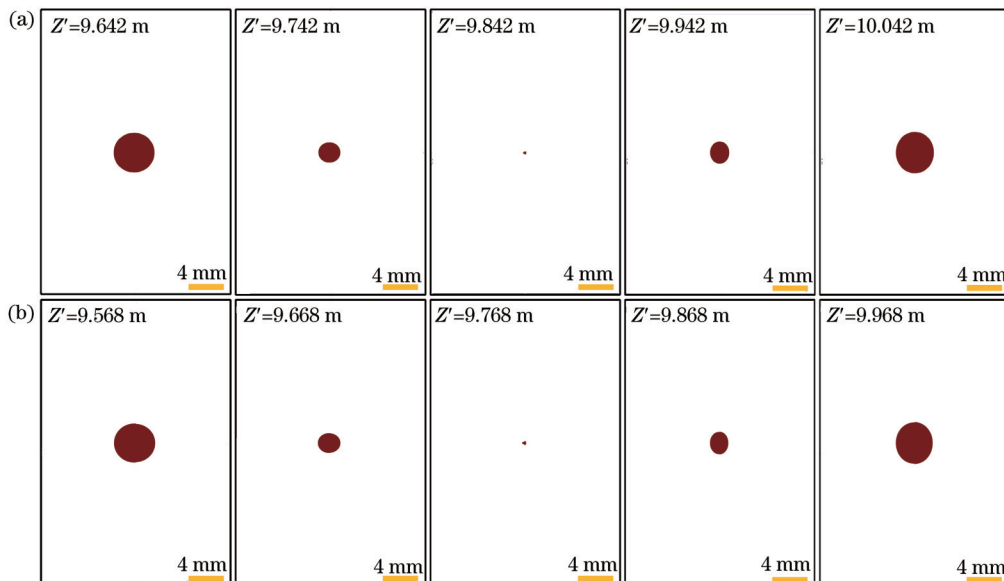


图 12 引入水平方向和坚直方向矢高误差下距离凹面镜不同位置处的光斑图。(a) 水平方向;(b) 坚直方向

Fig. 12 Light spot patterns at different positions from concave mirror with introduced horizontal and vertical Sag errors. (a) Horizontal direction; (b) vertical direction

对比图 7 仿真结果, 在分别引入水平方向和坚直方向矢高误差后, 系统的聚焦位置均略有前移, 在焦点前后处光斑略呈椭圆状, 光斑规则度均降低, 且导致聚焦时的光斑半径分别增大至 $95 \mu\text{m}$ 和 $140 \mu\text{m}$ 。因此, 依据上述分析结果可以预测, 由于较大的加工误差, 故实验上系统像差的补偿效果将差于仿真结

果, 聚焦位置会提前, 且聚焦时的光斑半径将大于仿真结果。

5.2 像差补偿实验

为了研究相位板实际补偿效果, 将透射式自由曲面相位板按照设计位置和角度摆放在光路中, 并进一步严格精细装调, 实验光路示意图如图 13 所示。

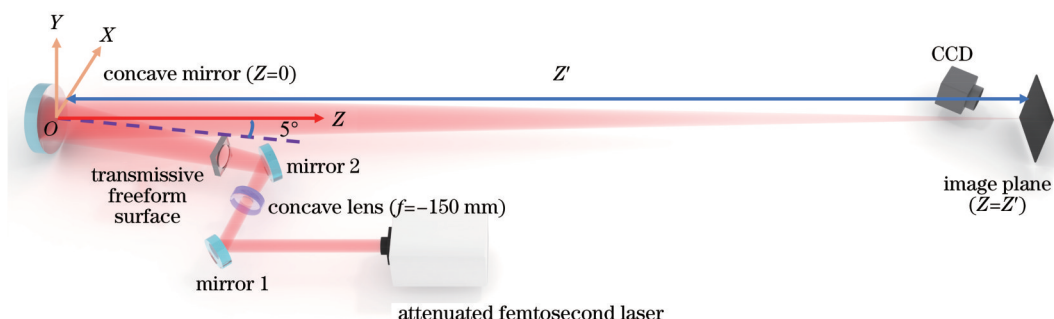


图 13 透射式自由曲面相位板像差补偿光路示意图

Fig. 13 Schematic diagram of optical path for aberration compensation by transmission freeform surface phase plate

飞秒激光的中心波长为 800 nm , 脉冲宽度为 60 fs , 重复频率为 500 Hz , 最高单脉冲能量为 4 mJ , 初始束腰半径为 4 mm 。首先, 为了较为直观地对比, 减小了飞秒激光的能量, 此时激光的非线性效应很弱, 以线性传输为主, 分别记录像差补偿前后 10 m 聚焦处及

其前后位置的光斑图, 如图 14 和图 15 所示。

对比图 14 和图 15 的光斑形状和光斑大小能够发现, 透射式自由曲面相位板具有非常良好的实际像差补偿效果。为了进一步量化比较补偿前后聚焦光斑的大小, 在与凹面镜相距 $9.64 \sim 10.34 \text{ m}$ 范围内, 计算了

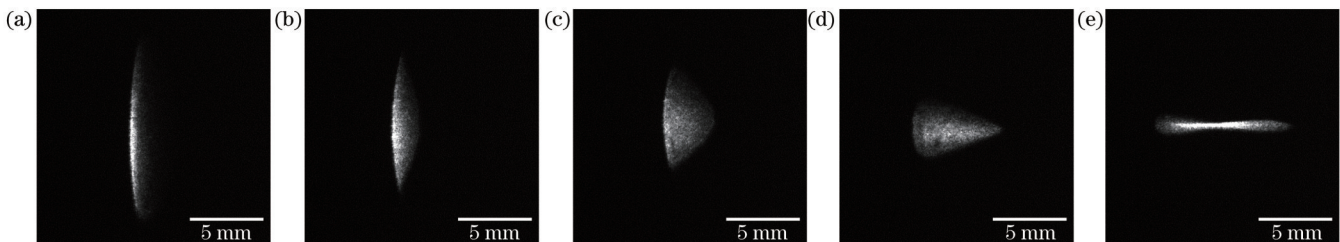


图14 实验中CCD拍摄到补偿前与凹面反射镜不同距离处的光斑图。(a) $Z'=9.8\text{ m}$; (b) $Z'=9.9\text{ m}$; (c) $Z'=10.0\text{ m}$; (d) $Z'=10.1\text{ m}$; (e) $Z'=10.2\text{ m}$

Fig. 14 Spot patterns at different distances from concave mirror captured by CCD in experiment before compensation. (a) $Z'=9.8\text{ m}$; (b) $Z'=9.9\text{ m}$; (c) $Z'=10.0\text{ m}$; (d) $Z'=10.1\text{ m}$; (e) $Z'=10.2\text{ m}$

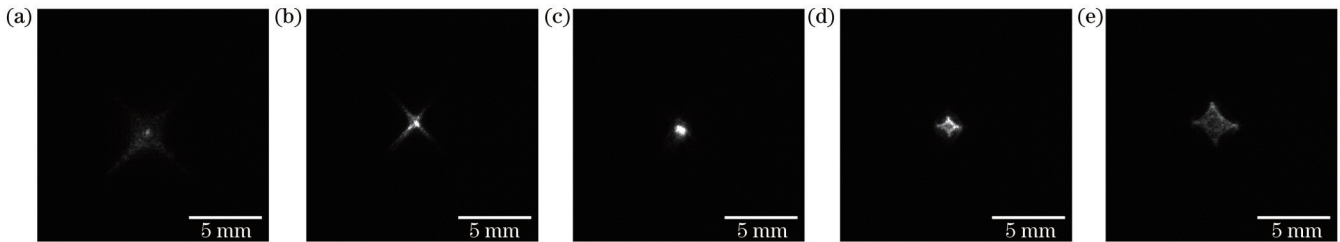


图15 实验中CCD拍摄到补偿后与凹面反射镜不同距离处的光斑图。(a) $Z'=9.3\text{ m}$; (b) $Z'=9.4\text{ m}$; (c) $Z'=9.5\text{ m}$; (d) $Z'=9.6\text{ m}$; (e) $Z'=9.7\text{ m}$

Fig. 15 Spot patterns at different distances from concave mirror captured by CCD in experiment after compensation. (a) $Z'=9.3\text{ m}$; (b) $Z'=9.4\text{ m}$; (c) $Z'=9.5\text{ m}$; (d) $Z'=9.6\text{ m}$; (e) $Z'=9.7\text{ m}$

不同位置处以光斑质心作为参考的RMS半径大小,结果如图16所示。

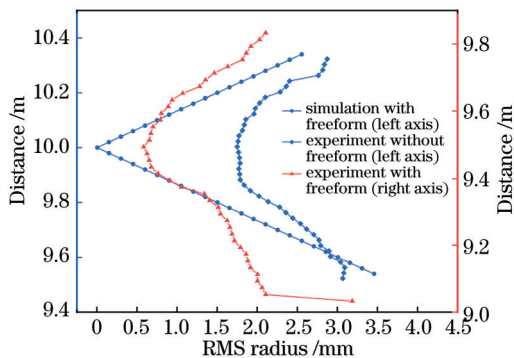


图16 像差补偿前后飞秒激光聚焦光斑的RMS半径曲线
Fig. 16 RMS radius curves of femtosecond laser focusing spot before and after aberration compensation

从图16可以看出,引入相位板后,实验中聚焦位置偏离理论值,前移至距凹面镜约9.50 m处。相比于像差补偿前的实验结果,补偿后光斑尺寸均有明显减小,尤其在聚焦位置处,聚焦光斑RMS半径由补偿像差前的约1.75 mm减小至补偿像差后小于0.50 mm。相比于仿真结果,实验中像差补偿后远离聚焦位置的光斑半径偏小,而在聚焦位置附近的光斑半径偏大。

为了进一步分析像差补偿前后飞秒激光聚焦光斑质量对光丝强度的影响,提升飞秒激光能量,此时产生光丝非线性效应,采用超声波探测法对光丝强度^[26-27]

进行表征。图17展示了光丝的超声信号强度分布变化曲线。可以看到:在利用透射式自由曲面相位板补偿系统像差后,聚焦位置光丝的超声信号强度提高近56倍;像差补偿前的曲线显示其存在两个超声强度峰值,而补偿后只存在一个超声强度峰,这也很好地证明了透射式自由曲面相位板对原实验系统中的像散像差具有良好的补偿效果,能够显著提高光丝强度。

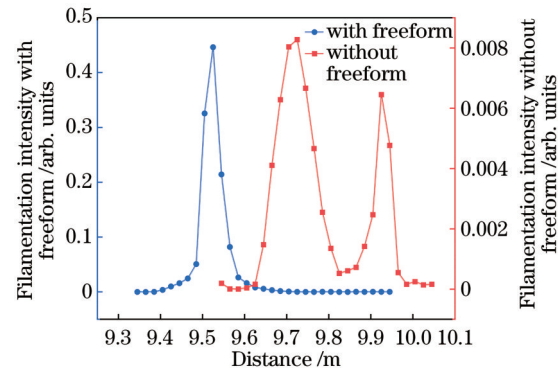


图17 使用超声探测方法对飞秒激光成丝系统像差补偿前后光丝强度的表征结果

Fig. 17 Characterization results of filamentation intensities of femtosecond laser filamentation system before and after aberration compensation using ultrasonic detection method

6 讨论与分析

在图13所示的实验系统中,由于相位板存在加工

和装调误差,故势必会引起实验中不同聚焦位置处的光斑尺寸大于理论仿真值,但图16所示实验结果中,光斑尺寸在远离聚焦位置和在聚焦位置附近处相对于仿真结果呈现不同的变化规律。出现该现象的原因在于远离聚焦位置的光斑能量分布更为弥散,导致对光斑图像进行预处理并确定质心的图像处理算法因光斑边缘能量的弥散使计算所得的光斑尺寸明显小于实际值,其偏差甚至超过了器件和系统误差对光斑尺寸的影响。在聚焦位置附近,由于光斑能量更为集中,故图像处理算法计算所得的光斑尺寸更加接近真实的光斑尺寸,该计算值与仿真值的偏差主要由相位板加工和装调误差决定,印证了图12中加工误差会导致聚焦光斑尺寸偏大的预测。

相位板加工误差除了会影响聚焦时的光斑尺寸外,图12所示的仿真分析表明它还会使光束聚焦位置前移。在实验中,采用相位板补偿后,当飞秒激光在线性条件下传输时,光束聚焦位置相较于仿真的确存在前移现象,如图16所示。然而,当飞秒激光非线性传输时,所形成的光丝不仅会因自聚焦效应而移动到光束聚焦位置之前^[28],还会因相位板面形加工误差的影响而进一步前移,如图17所示。

虽然引入相位板补偿后加工误差会导致光丝位置偏离理论设计预期,但是系统像差得到了一定的程度补偿,故光丝强度相较于补偿前仍有明显的增强,如图17所示。这充分验证了飞秒激光成丝系统中引入自由曲面相位板对提升荧光探测灵敏度的有效性。同时,该方法也适用于飞秒激光成丝于千米级距离时因能量进一步提升而产生多丝的情形。研究表明,多丝现象有利于提高远距离荧光探测灵敏度^[29]。相较于提升单丝强度的相位板,在设计针对多丝现象的相位板时,可将改善光束聚焦时光斑质量和能量空间分布特性作为主要优化目标,在聚焦平面上产生多个“热点”,便于产生多根光丝,从而提高补偿后系统的荧光探测效率。

7 结 论

针对远距离飞秒激光聚焦成丝系统中主要存在的像散像差,采用了基于18项Fringe Zernike多项式表征的透射式自由曲面相位板进行补偿。经过优化设计之后,系统中的像差得到了有效补偿。对设计结果进行了包括面形和装调公差在内的公差分析,并进行了器件的加工。为了验证其在实验系统中的像差补偿效果,将加工后的自由曲面按照设计装调至光路中:在飞秒激光线性传输条件下,聚焦时的光斑形状规则,在聚焦位置处光斑的RMS半径小于0.5 mm,聚焦光斑质量良好;在非线性传输条件下,采用超声波探测法对形成的光丝强度进行表征,像差补偿后超声信号强度提高了56倍。因此,使用光学自由曲面补偿飞秒激光成丝系统中的像差具有较强的可行性,特别是在保证一

定加工精度和装调精度的条件下,自由曲面相位板将具有非常好的像差补偿效果,对于增强远距离飞秒激光成丝强度和提升其遥感探测灵敏度具有很好的实用价值。

参 考 文 献

- [1] Zhu Z M, Yao P Q, Zheng W H. Design of a free-form surface microlens array optical system with high efficiency and uniformity [J]. Applied Optics, 2020, 59(23): 6939-6944.
- [2] Reimers J, Bauer A, Thompson K P, et al. Freeform spectrometer enabling increased compactness[J]. Light: Science & Applications, 2017, 6(7): e17026.
- [3] Reshidko D, Sasian J. Method for the design of nonaxially symmetric optical systems using free-form surfaces[J]. Optical Engineering, 2018, 57(10): 101704.
- [4] 杨通, 段璎哲, 程德文, 等. 自由曲面成像光学系统设计: 理论、发展与应用[J]. 光学学报, 2021, 41(1): 0108001.
- [5] Yang T, Duan Y Z, Cheng D W, et al. Freeform imaging optical system design: theories, development, and applications [J]. Acta Optica Sinica, 2021, 41(1): 0108001.
- [6] Zhu D Y, Chen Y, Hu Z J, et al. Experimental study on measurement of free-form surface with wavefront reconstruction algorithm[J]. Infrared Physics & Technology, 2021, 115: 103671.
- [7] 李杰, 罗辉, 李金铖, 等. 基于谐衍射与自由曲面的机载红外双波段成像光学系统设计[J]. 光子学报, 2021, 50(12): 1222004.
- [8] Li J, Luo H, Li J C, et al. Design of airborne infrared dual-band imaging optical system based on harmonic diffraction and free-form surface[J]. Acta Photonica Sinica, 2021, 50(12): 1222004.
- [9] 张艺蓝, 史浩东, 王超, 等. 离轴自由曲面光学系统偏振像差特性研究[J]. 光学学报, 2021, 41(18): 1822002.
- [10] Zhang Y L, Shi H D, Wang C, et al. Research on polarization aberration characteristics of off-axis freeform surface optical system[J]. Acta Optica Sinica, 2021, 41(18): 1822002.
- [11] 陈玉强, 张效栋, 刘现磊. 自由曲面成像系统的光学性能评价[J]. 光学学报, 2020, 40(24): 2412002.
- [12] Chen Y Q, Zhang X D, Liu X L. Evaluation of optical performance of free-form surface imaging system[J]. Acta Optica Sinica, 2020, 40(24): 2412002.
- [13] Chen B, Herkommer A M. Alternate optical designs for head-mounted displays with a wide field of view[J]. Applied Optics, 2017, 56(4): 901-906.
- [14] Cheng D W, Duan J X, Chen H L, et al. Freeform OST-HMD system with large exit pupil diameter and vision correction capability[J]. Photonics Research, 2022, 10(1): 21-32.
- [15] Jang C G, Mercier O, Bang K, et al. Design and fabrication of freeform holographic optical elements[J]. ACM Transactions on Graphics, 2020, 39(6): 184.
- [16] Nie Y F, Mohedano R, Benítez P, et al. Multifield direct design method for ultrashort throw ratio projection optics with two tailored mirrors[J]. Applied Optics, 2016, 55(14): 3794-3800.
- [17] Wei S L, Fan Z C, Zhu Z B, et al. Design of a head-up display based on freeform reflective systems for automotive applications [J]. Applied Optics, 2019, 58(7): 1675-1681.
- [18] 陈炳旭, 廖志远, 操超, 等. 大视场大相对孔径自由曲面成像系统设计[J]. 红外与激光工程, 2020, 49(8): 20200005.
- [19] Chen B X, Liao Z Y, Cao C, et al. Design of the freeform imaging system with large field of view and large relative aperture[J]. Infrared and Laser Engineering, 2020, 49(8): 20200005.
- [20] 李越强, 操超. 大视场高分辨率自由曲面成像光学系统设计[J]. 光学与光电技术, 2021, 19(6): 57-63.
- [21] Li Y Q, Cao C. Design of the freeform imaging optical system

- with large field of view and high resolution[J]. Optics & Optoelectronic Technology, 2021, 19(6): 57-63.
- [16] 李俊阳, 李文强, 龙龙, 等. 基于自由曲面的离轴三反光学系统设计方法研究[J]. 激光与光电子学进展, 2020, 57(9): 092202.
- Li J Y, Li W Q, Long Y, et al. Design of off-axis three-mirror optical system based on free-form surface[J]. Laser & Optoelectronics Progress, 2020, 57(9): 092202.
- [17] 李元, 李艳, 何玉兰, 等. 紧凑型自由曲面离轴三反系统设计[J]. 应用光学, 2018, 39(6): 780-784.
- Li Y, Li Y, He Y L, et al. Design of compact freeform off-axis three-mirror system[J]. Journal of Applied Optics, 2018, 39(6): 780-784.
- [18] Vallerotto G, Victoria M, Askins S, et al. Design and modeling of a cost-effective achromatic Fresnel lens for concentrating photovoltaics[J]. Optics Express, 2016, 24(18): A1245-A1256.
- [19] Yang Y S, Qiu D S, Zeng Y, et al. Design of a reflective LED automotive headlamp lighting system based on a free-form surface[J]. Applied Optics, 2021, 60(28): 8910-8914.
- [20] 张文裕, 苏宙平. 基于二维面形加权叠加的扩展LED光源自由曲面透镜设计[J]. 激光与光电子学进展, 2022, 59(11): 1122003.
- Zhang W Y, Su Z P. Design of free-form surface lens of extended LED light source based on two-dimensional surface shape weighted superposition[J]. Laser & Optoelectronics Progress, 2022, 59(11): 1122003.
- [21] 段文举, 朴明旭, 全向前, 等. 适于扩展光源的紧凑型双自由曲面匀光透镜设计[J]. 光学学报, 2022, 42(15): 1522001.
- Duan W J, Piao M X, Quan X Q, et al. Design of compact double freeform surface lens with uniform illumination for extended light source[J]. Acta Optica Sinica, 2022, 42(15): 1522001.
- Su Q, Sun L, Chu C Y, et al. Effect of molecular orbital angular momentum on the spatial distribution of fluorescence during femtosecond laser filamentation in air[J]. The Journal of Physical Chemistry Letters, 2020, 11(3): 730-734.
- [23] Yuan S, Chen R L, Zeng H P. Femtosecond filamentation induced fluorescence technique for atmospheric sensing[J]. Chinese Physics B, 2015, 24(1): 014208.
- [24] Wu J B, Wu Z Y, Chen T, et al. Spatial distribution of the fluorescence induced by femtosecond laser filamentation in ambient air[J]. Optics & Laser Technology, 2020, 131: 106417.
- [25] Andrianov K Y, Kandidov V P, Kosareva O G, et al. Influence of beam quality on filamentation of high-power femtosecond laser pulses in air[C]//17th International Conference on Coherent and Nonlinear Optics (Icono-2001), June 26-July 1, 2001, Minsk, Belarus, Russia. Moscow: Mezhdunarodnaya Kniga, 2001, 66(3): 1091-1102.
- [26] 刘伟伟, 薛嘉云, 苏强, 等. 超快激光成丝现象研究综述[J]. 中国激光, 2020, 47(5): 0500003.
- Liu W W, Xue J Y, Su Q, et al. Research progress on ultrafast laser filamentation[J]. Chinese Journal of Lasers, 2020, 47(5): 0500003.
- [27] Yu J, Mondelain D, Kasparian J, et al. Sonographic probing of laser filaments in air[J]. Applied Optics, 2003, 42(36): 7117-7120.
- [28] Marburger J H. Self-focusing: theory[J]. Progress in Quantum Electronics, 1975, 4: 35-110.
- [29] Chu C Y, Zhang Z, Sun L, et al. Raising the saturation point of fluorescence emitted by air optical filament via π phase plate[J]. Optical Engineering, 2021, 60(7): 076105.

Application of Freeform Surface in Aberration Compensation of Femtosecond Laser Filamentation System

Xie Bofu¹, Zhao Xing^{1,2*}, Tao Shishi¹, Zhang Shuai¹, Li Haoran¹, Li Yuanbo¹, Liu Hongliang^{1,2}, Liu Weiwei^{1,2}

¹Institute of Modern Optics, Nankai University, Tianjin 300350, China;

²Tianjin Key Laboratory of Micro-scale Optical Information Science and Technology, Tianjin 300350, China

Abstract

Objective High-power ultrafast femtosecond laser will form a unique plasma channel at the beam focus due to the nonlinear effect when propagating in a transparent optical medium, namely, filamentation. Filamentation can be used as the excitation source of the fluorescence spectrum for detecting material components, which is of great application value in monitoring atmospheric pollutants. However, when the optical system is used to remotely focus a femtosecond laser into a filament, the aberration in the system can lead to the irregular shape of the focused light spot, as well as a larger radius and poorer quality. As a result, filamentation intensity is weakened, and the detection sensitivity of the system is reduced, which is not conducive to remote detection of atmospheric pollutants with a low concentration. Therefore, determining how to effectively reduce the aberration of the femtosecond laser filamentation system and improve the quality of the focused light spot is essential for enhancing the filamentation intensity and the detection sensitivity of the system.

Methods On the basis of the strong aberration compensation ability of the optical freeform surface, we propose a method introducing a transmission freeform surface phase plate into the femtosecond laser filamentation system to compensate for the system aberration. Firstly, by simulating and analyzing the aberration characteristics of the original system in the optical design software, we design the compensation freeform surface phase plate to reduce some main aberrations and overall wave-front aberrations. The results of the optimal design show that the system aberration is significantly reduced,

and the light spot has a more regular shape and a smaller size. Then, we investigate the manufacturability of the designed freeform surface phase plate by tolerance analysis and manufacture the phase plate by single-point diamond turning successfully. Finally, we adjust the femtosecond laser filamentation system with a freeform surface phase plate and carry out the laser filamentation experiment. The experimental results demonstrate the effectiveness of the freeform surface phase plate, with the shape regularity of the focused light spot improved and its radius significantly reduced, and filamentation intensity of femtosecond laser filamentation system is greatly enhanced.

Results and Discussions Firstly, a freeform surface phase plate is optimized in CODE V to compensate for the aberration of the femtosecond laser filamentation system when the laser is focused at 10 m. The shape of the focused light spot is more regular, and its radius is reduced after optimization (Fig. 7), which means the main aberration of the system, astigmatism in the X direction, and the overall wave-front aberration are greatly decreased (Fig. 8). Secondly, after the tolerance analysis of the designed freeform surface phase plate (Fig. 9), the phase plate is manufactured by single-point diamond turning. Then, the horizontal and vertical surface shapes of the phase plate are scanned by ZYGO's profilometer, and manufacturing errors in both directions can be achieved (Fig. 11). These errors can be converted into curvature radius changes to analyze the influence on the compensation results (Fig. 12). According to the analysis results, the performance of aberration compensation in experiments are predicted. The phase plate is installed in the original system to study the aberration compensation experimentally. The light spot images in the experiment show that the shape regularity of the compensated light spot is effectively improved, and its radius is significantly reduced (Fig. 15). However, due to the manufacturing error of the phase plate surface, the actual radius of the compensated light spot is larger than the simulation result, and the focusing position moves forward (Fig. 16), which confirms the previous prediction results. Finally, ultrasonic signals are used to characterize the filament intensity before and after compensation. The results show that the filamentation intensity after compensation is 56 times higher than that before compensation (Fig. 17).

Conclusions In this paper, the transmissive freeform surface phase plate is used to compensate for the astigmatic aberration mainly existing in the femtosecond laser filamentation system. After the optimal design, the aberration in the system has been effectively compensated. The tolerance analysis of the design results, including surface shape and assembly and adjustment tolerance, is carried out, and the device is manufactured. The manufactured freeform surface is set into the system according to the design to verify its aberration compensation effect in the experiment. The light spot shape during focusing is more regular, and the RMS radius of the light spot at the focusing position is less than 0.5 mm when the femtosecond laser propagates linearly. Moreover, the ultrasonic signal intensity, which is utilized to characterize the filamentation intensity, is 56 times higher than the case when femtosecond laser propagates nonlinearly. Therefore, it is feasible to use optical freeform surfaces to compensate for the aberration in the femtosecond laser filamentation system, which is of great practical value for enhancing the filamentation intensity of femtosecond laser filamentation system at a long distance and improving its remote sensing detection sensitivity.

Key words optical design; aberration compensation; femtosecond laser filamentation; optical freeform surface